



This is a repository copy of *On the performance of indoor multi-storey small-cell networks*.

White Rose Research Online URL for this paper:
<https://eprints.whiterose.ac.uk/166735/>

Version: Accepted Version

Article:

Chen, C., Zhang, Y., Zhang, J. et al. (2 more authors) (2021) On the performance of indoor multi-storey small-cell networks. *IEEE Transactions on Wireless Communications*, 20 (2). pp. 1336-1348. ISSN 1536-1276

<https://doi.org/10.1109/TWC.2020.3032740>

© 2020 IEEE. Personal use of this material is permitted. Permission from IEEE must be obtained for all other users, including reprinting/ republishing this material for advertising or promotional purposes, creating new collective works for resale or redistribution to servers or lists, or reuse of any copyrighted components of this work in other works. Reproduced in accordance with the publisher's self-archiving policy.

Reuse

Items deposited in White Rose Research Online are protected by copyright, with all rights reserved unless indicated otherwise. They may be downloaded and/or printed for private study, or other acts as permitted by national copyright laws. The publisher or other rights holders may allow further reproduction and re-use of the full text version. This is indicated by the licence information on the White Rose Research Online record for the item.

Takedown

If you consider content in White Rose Research Online to be in breach of UK law, please notify us by emailing eprints@whiterose.ac.uk including the URL of the record and the reason for the withdrawal request.



eprints@whiterose.ac.uk
<https://eprints.whiterose.ac.uk/>

On the Performance of Indoor Multi-storey Small-cell Networks

Chen Chen, *Student Member, IEEE*, Yixin Zhang, *Student Member, IEEE*, Jiliang Zhang, *Senior Member, IEEE*, Xiaoli Chu, *Senior Member, IEEE*, Jie Zhang, *Senior Member, IEEE*

Abstract—Mobile data traffic has been largely generated indoors. However, indoor cellular networks have been studied either on a two-dimensional (2D) plane or as an intractable optimization problem for a multi-storey building. In this paper, we develop a tractable three-dimensional small-cell network model for a multi-storey building. On each storey, the small-cell base stations (BS) are distributed following a 2D homogeneous Poisson point process. We analytically derive the downlink coverage probability, spectral efficiency (SE) and area spectral efficiency for the indoor network as functions of the storey height, the penetration loss of the ceiling and the BS density. Our tractable expressions show that a higher penetration loss of the ceiling leads to a higher coverage probability and a higher SE. Meanwhile, with the increase of the storey height or the BS density, the downlink coverage probability first decreases and then increases after reaching a minimum value, indicating that certain values of storey height and BS density should be avoided for good indoor wireless coverage.

Index Terms—Indoor, small-cell networks, storey height, stochastic geometry, coverage probability, spectral efficiency.

I. INTRODUCTION

The fifth generation (5G) of mobile networks is predicted to support $1000\times$ mobile data traffic in the next decade [1]. According to [2] [3], approximately 80% of the mobile data is generated indoors, while over 70% of the indoor traffic is carried by the outdoor cellular networks. Since outdoor-to-indoor coverage is prone to suffer from the high penetration loss of walls and other physical obstacles, it is of high necessity to deploy indoor small-cell base stations (BS) [4] [5].

While the modelling and analysis of outdoor networks has been widely studied in recent years [6]–[11], there are still open questions regarding the performance of indoor cellular networks. The existing works mainly focus on the modelling of blockages including walls and random blockages on two-dimensional (2D) planes [12]–[17]. However, the study of indoor cellular networks in multi-storey buildings should not be limited to a 2D BS deployment.

In this paper, we present for the first time a tractable three-dimensional (3D) small-cell network (SCN) model for the multi-storey indoor environment by incorporating the storey height and the penetration loss of the ceiling. Then we derive the expressions for the coverage probability, spectral

efficiency (SE) and area spectral efficiency (ASE) where the user equipment (UE) association and inter-cell interference are considered. We analyze the effects of the storey height and the penetration loss of the ceiling on the coverage probability and SE, and provide useful guidelines for the indoor small-cell deployment and the design of a new building from the perspective of wireless communications [37].

A. Related Works

Stochastic geometry has been widely used to analyze the performance of cellular networks due to its mathematical tractability [18]–[22]. It was also employed to model networks for the indoor built environment, e.g. in [14], where the authors modeled the BSs and the center points of the walls as two independent homogeneous Poisson point process (PPP). The results showed that higher interior-wall attenuation values can provide higher coverage probability due to the reduced inter-cell interference. In [13], a binomial point process was adopted to model a finite-sized indoor network. Considering the larger antenna arrays and shorter transmission distances of millimeter wave (mm-Wave) networks, the authors assumed a triangle transmitter-receiver radiation area involving the effects of random blockages and calculated the bit error rate and outage probability. However, these works only considered a 2D BS deployment.

The authors of [23] extended the 2D PPP distribution of BSs to the 3D space with BS density in BSs/m^3 and employed the free space path loss channel model. It was shown that the 3D cellular network achieved a lower coverage probability compared with the traditional 2D models, but the influence of the BS density was not analyzed. In [24], the dual-slope path loss model was applied in a 3D PPP model. The asymptotic analysis showed that the coverage probability would diminish to zero when the density of BSs goes to infinity. In [25], a 3D Poisson building model was proposed to model the correlated indoor shadowing. However, these 3D models cannot be applied to SCNs in the multi-storey in-building scenarios, where BSs on the same storey usually have the same height for the sake of simple deployment.

Most existing works on multi-storey BS deployment focused on some specific optimization problems [26]–[28]. For instance, the authors of [26] optimized the BS placement taking into account the power control. After reformulating the mixed-integer nonconvex problem into a convex problem, the optimal number and locations of the BSs were obtained. Nevertheless, no tractable models have been proposed to analyze SCNs in the multi-storey building scenarios.

Dense deployment of SCN is considered as one of the key techniques of 5G networks [32]. The traditional understanding

Chen Chen, Yixin Zhang, Jiliang Zhang and Xiaoli Chu are with Department of Electronic and Electrical Engineering, The University of Sheffield, Sheffield, S1 4ET, United Kingdom. Jie Zhang is with the Department of Electronic and Electrical Engineering, the University of Sheffield, Sheffield, S1 4ET, UK, and also with Ranplan Wireless Network Design Ltd., Cambridge, CB23 3UY, UK.

This project has received funding from the European Union Horizon 2020 research and innovation program under the Marie Skłodowska-Curie grant agreement No. 766231 WAVE-COMBE H2020-MSCA-ITN-2017.

of network densification is that the increase of BS density does not change the coverage probability of the typical UE in an interference limiting scenario [18] [29]. This conclusion indicates that the area spectral efficiency scales linearly with the BS density, namely the capacity gain can always be obtained. However, it is worth noting that this result is based on the simplified free space propagation channel model. Considering the short-range propagation in dense SCNs, the authors in [30] [31] proposed a bounded path loss model and showed that the ultra dense network degrades the spatial throughput. In [33], a multi-slope path loss model was employed to study the effect of non-line-of-sight transmission on the coverage probability. Their results showed that when the BS density increases above a certain value, the coverage probability starts to decrease and the increase in ASE slows down. In [34], the authors studied the effect of the height of BS antennas on the coverage probability and the ASE, which decrease to zero with the BS density when the BSs are higher than the UEs.

B. Contributions

In this paper, we study the performance of a 3D SCN in a multi-storey building. The main contributions of this paper are summarized as follows:

- We propose a novel 3D SCN model for a multi-storey building where BSs on each storey follow PPP distribution. Using tools from stochastic geometry, we derive the analytical expressions of coverage probability and SE for a building with $2M + 1$ storeys, where $M \geq 1$.
- Based on the results above, the numerically tractable integral expressions for the $M = 1$ case are obtained and validated by simulation results. The numerical results show that the $M = 1$ case shows similar performance in terms of coverage probability and SE as the $M > 1$ cases, therefore our analytical expressions for the $M = 1$ case can be used to numerically predict the coverage probability and SE of a SCN in a building with $2M + 1$ storeys, where $M \geq 1$.
- With our analytical results, we find that both the coverage probability and SE first decrease and then increase with the increasing storey height. Accordingly, we identify a range of storey heights associated with poor network performance that should be avoided in the design of a new building. Moreover, our results show that both the coverage probability and SE first decrease and then increase with the BS density on each storey. This new finding is different from previous results obtained under the 2D scenarios [18] [19]. It indicates that the setting of BS density per storey in a multi-storey building should avoid the values that result in poor coverage.

C. Paper Organization

The remainder of this paper is structured as follows. Section II introduces the system model. Section III gives the analytical results on the coverage probability. Section IV presents the analytical results on the spectral efficiency. The numerical results are discussed in Section V, with remarks shedding some new light on the deployment of dense SCN. Finally, the conclusions are drawn in Section VI.

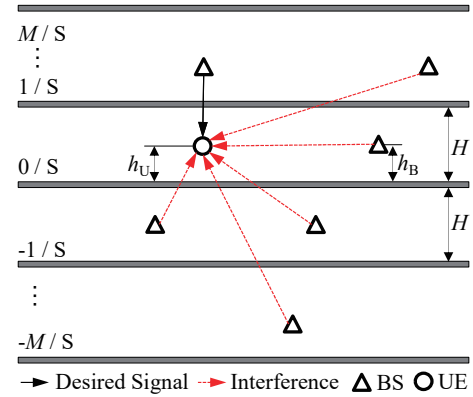


Fig. 1. An illustration of the small-cell network in a multi-storey building.

TABLE I
SUMMARY OF NOTATIONS

Notation	Meaning
m	Index of the storey where $m \in \{-M, \dots, 0, \dots, M\}$
Φ_j	Set of BSs on the j th storey
λ	Density of BSs on each storey
h_B	Height of BSs on each storey
h_U	Height of UEs on each storey
H	Height of each storey
P	Transmit power of BSs
α	Path loss exponent of each storey
T	Coverage probability threshold
w	Penetration loss of one ceiling
N	Additive white Gaussian noise power
β_0	Path loss at the reference distance
R_m	Horizontal distance from the typical UE to the nearest BS on the m th storey
l_m	Distance from the typical UE to the nearest BS on the m th storey
$P_{r,m}$	Average power of the strongest received signal from a BS on the m th storey
\mathcal{B}_m	Probability that the typical UE is associated to a BS on the m th storey
\mathcal{C}_m	Coverage probability when the typical UE is served by a BS on the m th storey
\mathcal{R}_m	Average ergodic rate when the typical UE is served by a BS on the m th storey
\mathcal{C}, \mathcal{R}	Coverage probability and average ergodic rate

II. SYSTEM MODEL

We consider a building with $2M + 1$ storeys, where $M \geq 1$. Table I presents a summary of notations used. As shown in Fig. 1, all the storeys from the ground storey to the top storey are numbered from $-M$ to M , respectively, and we assume that the typical UE is located on the 0th storey. The BS height and the UE height are assumed to be h_B and h_U , respectively. The height for each storey is denoted by H , which includes the ceiling height and the ceiling thickness. For the j th storey, the small-cell BSs are randomly distributed following a homogeneous PPP Φ_j with intensity λ BSs/m² and UEs are also PPP distributed with a density of ρ UEs/m². For simplicity, we assume that the values of λ and ρ do not change across different storeys. In this work, we adopt PPP to model the BSs on each storey mainly for its higher analytical tractability as compared with other point processes (such as

binomial point process and Poisson cluster process).

For the downlink cellular network, we assume that the desired and interference signals experience the distance dependent path loss, where the same path loss exponent α is used for all the storeys. Small scale fading is modeled as Rayleigh fading with an unit average power for all the channels [33], [35].

The simulation results in Fig. 3 in Section V will show that the maximum coverage probability is obtained when the BS height is the same as the UE height. For analytical tractability in the following, we assume that on each storey, $h_B = h_U$. Note that under this assumption, the value of h_B and h_U has no effect on the coverage probability.

One UE can only be associated to one BS. We use $m \in \{-M, -(M-1), \dots, 0, 1, \dots, M\}$ as the index of the storey that contains the serving BS for the typical UE. Let R_m denote the horizontal distance from the nearest BS on the m th storey to the typical UE, and then the distance from the nearest BS on the m th storey to the typical UE is given by

$$l_m = \sqrt{(mH)^2 + R_m^2}. \quad (1)$$

The UE is associated to the BS providing the strongest downlink received signal. The average power of the strongest received signal from a BS on the m th storey is given by [12] [36]

$$P_{r,m} = P\beta_0 l_m^{-\alpha} w^{|m|}, \quad (2)$$

where P is the transmit power of a BS, β_0 is the path loss at the reference distance of 1 m, w ($0 < w < 1$) is the penetration loss of one ceiling, and the power of the small scale fading is averaged to be 1.

We denote the probability that the typical UE is associated to a BS on the m th storey as \mathcal{B}_m , and denote the horizontal distance from the typical UE to its serving BS as X_m . The following lemma gives the expression for the probability density function (PDF) of X_m , which will be useful for the derivations of the coverage probability in Section III. In our system model as defined in Fig. 1, the PDF for the m th storey is the same as that for the $-m$ th storey. In the following, we will focus on $0 \leq m \leq M$.

Lemma 1. *The PDF of the distance X_m between a typical UE and its serving BS is*

$$f_{X_m}(x) = \begin{cases} f_{X_{m,m}}(x), & 0 < x \leq I_{m,(m+1)}, \\ \dots \\ f_{X_{m,k}}(x), & I_{m,k} < x \leq I_{m,(k+1)}, \\ \dots \\ f_{X_{m,M}}(x), & I_{m,M} < x < \infty, \end{cases} \quad (3)$$

where $I_{m,k}$ is formulated as

$$I_{m,k} = \begin{cases} \sqrt{(kH)^2 w^{\frac{2(m-k)}{\alpha}} - (mH)^2}, & m \leq k \leq M \\ \infty, & k = M + 1 \end{cases} \quad (4)$$

and $f_{X_{m,k}}(x)$ is

$$f_{X_{m,k}}(x) = \frac{2\pi\lambda}{\mathcal{B}_m} x \exp\left\{-\pi\lambda(F_m + F_{m,k})\right\}, \quad (5)$$

where F_m and $F_{m,k}$ are given in (6), (7) in the next page.

Proof: See Appendix A. ■

III. COVERAGE PROBABILITY

The coverage probability \mathcal{C} is the probability that the SINR of the typical UE is higher than a target threshold. The typical UE can be connected to at most one BS, so the coverage probability is given by

$$\mathcal{C} = \sum_{m=-M}^M \mathcal{C}_m \mathcal{B}_m, \quad (8)$$

where \mathcal{B}_m is the probability that the typical UE associates to the BS on the m th storey, and \mathcal{C}_m is the corresponding coverage probability. Since $\mathcal{C}_m = \mathcal{C}_{-m}$, for clarity, we consider $0 \leq m \leq M$, \mathcal{C} will be

$$\mathcal{C} = \mathcal{C}_0 \mathcal{B}_0 + 2 \sum_{m=1}^M \mathcal{C}_m \mathcal{B}_m. \quad (9)$$

The typical UE is in coverage when its SINR from its associated BS is larger than the given threshold T , when the typical UE associates to the BS on the m th storey, the coverage probability averaged over the plane is

$$\mathcal{C}_m = \mathbb{E}_x [\mathbb{P}[\text{SINR}_m(x) > T]], \quad (10)$$

where x is the horizontal distance from the typical UE to its serving BS and SINR_m is denoted as

$$\text{SINR}_m = \frac{Pg_{m,0}(m^2 H^2 + x^2)^{-\frac{\alpha}{2}} w^m}{\sum_{j=-M}^M \sum_{i \in \Phi_j \setminus \mathcal{B}_{m0}} P h_{j,i} |Y_{ji}|^{-\alpha} w^{|j|} + \frac{N}{\beta_0}}, \quad (11)$$

where $g_{m,0}$ is the Raleigh fading with an unit average power, \mathcal{B}_{m0} denotes the serving BS, $h_{j,i}$ is the Raleigh fading power gain with unit mean from the interfering BS i on the j th storey, and $|Y_{ji}|$ is the distance between the interfering BS i on the j th storey and the typical UE, and N is the additive white Gaussian noise with a constant mean power.

A. General Case and Main Result

We first give the general result of the coverage probability and then analyze the special case of $M = 1$.

Theorem 1. *The coverage probability of the typical UE associated to the BS on the m th storey \mathcal{C}_m can be computed as*

$$\mathcal{C}_m = \sum_{k=m}^M \mathcal{C}_{m,k}, \quad (12)$$

where

$$\begin{aligned} \mathcal{C}_{m,k} = & \frac{2\pi\lambda}{\mathcal{B}_m} \int_{I_{m,k}}^{I_{m,(k+1)}} x \exp\left\{-\frac{T}{\text{SNR}_m}\right. \\ & \left. - \pi\lambda(F_m + F_{m,k}) - \pi\lambda \mathcal{Q}(m^2 H^2 + x^2) w^{-\frac{2m}{\alpha}}\right. \\ & \left. - 2\pi\lambda(m^2 H^2 + x^2) \sum_{n=1}^M \mathcal{Q}_{m,n,k} w^{\frac{2}{\alpha}(n-m)}\right\} dx, \end{aligned} \quad (13)$$

in (13), $I_{m,k}$, F_m , $F_{m,k}$ are defined in (4), (6), (7), respectively,

$$\text{SNR}_m = \frac{Pw^m \beta_0 (m^2 H^2 + x^2)^{-\frac{\alpha}{2}}}{N}, \quad (14)$$

and

$$\mathcal{Q} = \frac{2T}{\alpha - 2} {}_2F_1 \left[1, 1 - \frac{2}{\alpha}; 2 - \frac{2}{\alpha}; -T \right], \quad (15)$$

$$\mathcal{Q}_{m,n,k} = \begin{cases} \mathcal{Q}, & n \leq k \\ \frac{2TB_{m,n,x}^{2/\alpha-1}}{\alpha-2} {}_2F_1 \left[1, 1 - \frac{2}{\alpha}; 2 - \frac{2}{\alpha}; -\frac{T}{B_{m,n,x}} \right], & n > k \end{cases}, \quad (16)$$

where $B_{m,n,x} = (nH)^\alpha w^{m-n} (m^2 H^2 + x^2)^{-\frac{\alpha}{2}}$.

Proof: See Appendix B. ■

B. Special Case: $M = 1$

Fig. 2 shows the coverage probability versus the SINR threshold, it can be observed that the difference between the coverage probability of the $M = 1$ case and $M > 1$ cases is negligible. Therefore, the coverage probability of the $M = 1$ case can be used to predict that of cases with $M > 1$.

Proposition 1. When $M=1$, the coverage probability of the typical UE is

$$\mathcal{C}^{M=1} = \mathcal{B}_0 \mathcal{C}_0 + 2\mathcal{B}_1 \mathcal{C}_1 \quad (17)$$

where $\mathcal{B}_0 \mathcal{C}_0$ and $\mathcal{B}_1 \mathcal{C}_1$ can be found in (18), (19), and

$$\begin{aligned} \mathcal{Q}_{0,1} &= \frac{2TH^{-2}w^{\frac{2}{\alpha}}x^2}{\alpha-2} {}_2F_1 \left[1, 1 - \frac{2}{\alpha}; 2 - \frac{2}{\alpha}; -\frac{T}{H^\alpha w^{-1}x^{-\alpha}} \right]. \end{aligned} \quad (20)$$

Proof: The expression can be easily obtained by plugging $M = 1$ into (9). ■

Lemma 2. For an interference-limited network (where $N=0$), when $\lambda \rightarrow 0$, $\mathcal{C}^{M=1} = \mathcal{C}^{M=0}$, i.e., the coverage probability for a 3-storey 3D SCN will be identical to that for a single-storey 2D SCN.

Proof: From (17), it is clear that when $\lambda \rightarrow 0$, $\mathcal{B}_1 \mathcal{C}_1 = \frac{1}{(w^{-\frac{2}{\alpha}}+2)(\mathcal{Q}+1)}$, $\mathcal{B}_0 \mathcal{C}_0 = \frac{1}{(2w^{\frac{2}{\alpha}}+1)(\mathcal{Q}+1)}$, and thus $\mathcal{C}^{M=1} = \mathcal{B}_0 \mathcal{C}_0 + 2\mathcal{B}_1 \mathcal{C}_1 = \frac{1}{\mathcal{Q}+1} = \mathcal{C}^{M=0}$. ■

Lemma 3. For an interference-limited network (where $N=0$), when $H \rightarrow 0$ or $H \rightarrow \infty$, $\mathcal{C}^{M=1} = \mathcal{C}^{M=0}$, i.e., the coverage probability for a 3-storey 3D SCN is identical to that for a single-storey 2D SCN.

Proof: In (17), when $H \rightarrow 0$, $\mathcal{B}_1 \mathcal{C}_1 = \frac{1}{(w^{-\frac{2}{\alpha}}+2)(\mathcal{Q}+1)}$, $\mathcal{B}_0 \mathcal{C}_0 = \frac{1}{(2w^{\frac{2}{\alpha}}+1)(\mathcal{Q}+1)}$, and thus $\mathcal{C}^{M=1} = \frac{1}{\mathcal{Q}+1} = \mathcal{C}^{M=0}$. When $H \rightarrow \infty$, $\mathcal{B}_0 \mathcal{C}_0 = 2\pi\lambda \int_0^\infty x \exp\{-\pi\lambda x^2(\mathcal{Q}+1)\} dx = \frac{1}{\mathcal{Q}+1}$, $\mathcal{B}_1 \mathcal{C}_1 = 0$, and thus $\mathcal{C}^{M=1} = \frac{1}{\mathcal{Q}+1} = \mathcal{C}^{M=0}$. ■

$$F_m = 2 \left((m^2 H^2 + x^2) \frac{w^{-\frac{2}{\alpha}} (1 - w^{-\frac{2(m-1)}{\alpha}})}{1 - w^{-\frac{2}{\alpha}}} - \frac{(m-1)m(2m-1)}{6} H^2 \right) + (m^2 H^2 + x^2) w^{-\frac{2m}{\alpha}} + 2x^2, \quad (6)$$

$$F_{m,k} = 2 \left((m^2 H^2 + x^2) \frac{w^{\frac{2}{\alpha}} (1 - w^{\frac{2(k-m)}{\alpha}})}{1 - w^{\frac{2}{\alpha}}} - \frac{k(k+1)(2k+1) - m(m+1)(2m+1)}{6} H^2 \right), \quad (7)$$

$$\begin{aligned} \mathcal{B}_0 \mathcal{C}_0 &= 2\pi\lambda \int_0^{Hw^{-\frac{1}{\alpha}}} x \exp\left\{ -\frac{T}{\text{SNR}_0} - \pi\lambda x^2 \left(\mathcal{Q} + 2\mathcal{Q}_{0,1} w^{\frac{2}{\alpha}} + 1 \right) \right\} dx \\ &+ 2\pi\lambda \int_{Hw^{-\frac{1}{\alpha}}}^\infty x \exp\left\{ -\frac{T}{\text{SNR}_0} - \pi\lambda x^2 \left(\mathcal{Q} + 2\mathcal{Q} w^{\frac{2}{\alpha}} + 2w^{\frac{2}{\alpha}} - 2\frac{H^2}{x^2} + 1 \right) \right\} dx \\ &= 2\pi\lambda \int_0^{Hw^{-\frac{1}{\alpha}}} x \exp\left\{ -\frac{T}{\text{SNR}_0} - \pi\lambda x^2 \left(\mathcal{Q} + 2\mathcal{Q}_{0,1} w^{\frac{2}{\alpha}} + 1 \right) \right\} dx + \frac{\exp\left\{ -\frac{T}{\text{SNR}_0} - \pi\lambda H^2 \left(\mathcal{Q} w^{-\frac{2}{\alpha}} + 2\mathcal{Q} + w^{-\frac{2}{\alpha}} \right) \right\}}{(\mathcal{Q}+1)(2w^{\frac{2}{\alpha}}+1)}, \end{aligned} \quad (18)$$

$$\begin{aligned} \mathcal{B}_1 \mathcal{C}_1 &= 2\pi\lambda \int_0^\infty x \exp\left\{ -\frac{T}{\text{SNR}_1} - \pi\lambda \mathcal{Q} (H^2 + x^2) \left(w^{-\frac{2}{\alpha}} + 2 \right) - \pi\lambda \left(\frac{H^2 + x^2}{w^{\frac{2}{\alpha}}} + 2x^2 \right) \right\} dx \\ &= \frac{\exp\left\{ -\frac{T}{\text{SNR}_1} - \pi\lambda H^2 \left(\mathcal{Q} w^{-\frac{2}{\alpha}} + 2\mathcal{Q} + w^{-\frac{2}{\alpha}} \right) \right\}}{(w^{-\frac{2}{\alpha}}+2)(\mathcal{Q}+1)}, \end{aligned} \quad (19)$$

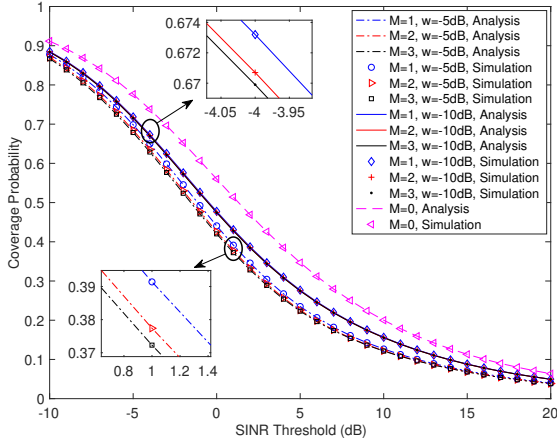
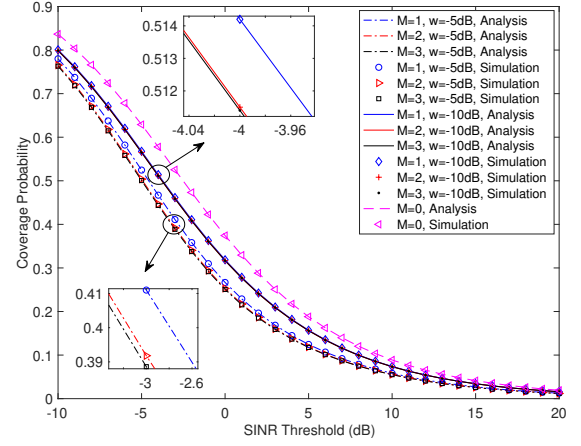
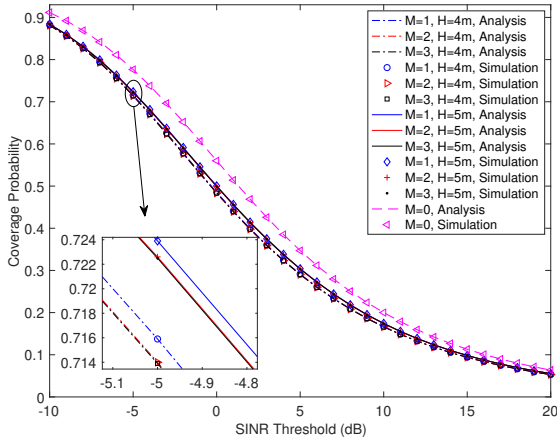
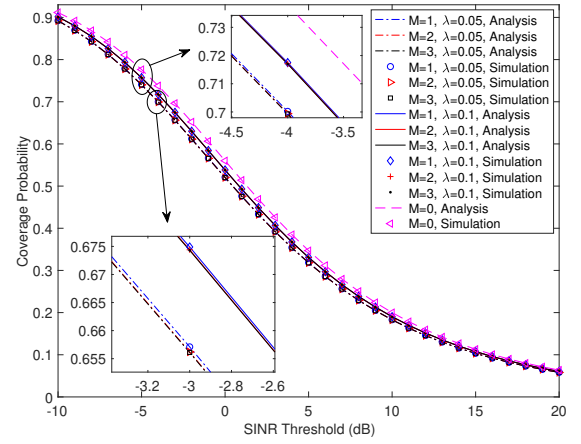

 (a) For different values of w and $\alpha = 4$.

 (b) For different values of w and $\alpha = 3$.

 (c) For different values of H .

 (d) For different values of λ (BS/m²).

 Fig. 2. Coverage probability vs. the SINR threshold for $M = 0, 1, 2$ and 3 .

IV. SPECTRAL EFFICIENCY

The spectral efficiency can be calculated using the average ergodic rate of the typical UE as follows

$$\mathcal{R} = \sum_{m=-M}^M \mathcal{R}_m \mathcal{B}_m, \quad (21)$$

where \mathcal{B}_m is the probability that the typical UE is associated to the BS on the m th storey. Similar to (9), (21) can be further rewritten as

$$\mathcal{R} = \mathcal{R}_0 \mathcal{B}_0 + 2 \sum_{m=1}^M \mathcal{R}_m \mathcal{B}_m, \quad (22)$$

\mathcal{R}_m is the average ergodic rate when the typical UE connects to the m th storey. \mathcal{R}_m can be derived as

$$\mathcal{R}_m = \mathbb{E}_{\text{SINR}_m} [\log_2 (1 + \text{SINR}_m)], \quad (23)$$

Theorem 2. The average ergodic rate of the m th storey can be derived as

$$\mathcal{R}_m = \sum_{k=m}^M \mathcal{R}_{m,k}, \quad (24)$$

where

$$\begin{aligned} \mathcal{R}_{m,k} = & \frac{2\pi\lambda}{\mathcal{B}_m} \int_0^\infty \int_{I_{m,k}}^{J_{m,(k+1)}} x \exp \left\{ -\frac{2^t - 1}{\text{SNR}_m} \right. \\ & - \pi\lambda (F_m + F_{m,k}) - \pi\lambda \mathcal{Q}_t (m^2 H^2 + x^2) w^{-\frac{2m}{\alpha}} \\ & \left. - 2\pi\lambda (m^2 H^2 + x^2) \sum_{n=1}^M \mathcal{Q}_{m,n,k,t} w^{\frac{2}{\alpha}(n-m)} \right\} dx dt, \end{aligned} \quad (25)$$

in which

$$\mathcal{Q}_t = \frac{2(2^t - 1)}{\alpha - 2} {}_2F_1 \left[1, 1 - \frac{2}{\alpha}; 2 - \frac{2}{\alpha}; 1 - 2^t \right], \quad (26)$$

$$\mathcal{Q}_{m,n,k,t} = \begin{cases} \mathcal{Q}_t, & n \leq k \\ \frac{2(2^t - 1) B_{m,n,x}^{2/\alpha - 1}}{\alpha - 2} {}_2F_1 \left[1, 1 - \frac{2}{\alpha}; 2 - \frac{2}{\alpha}; \frac{1 - 2^t}{B_{m,n,x}} \right], & n > k \end{cases} \quad (27)$$

where $B_{m,n,x} = (nH)^\alpha w^{-n} (m^2 H^2 + x^2)^{-\frac{\alpha}{2}}$.

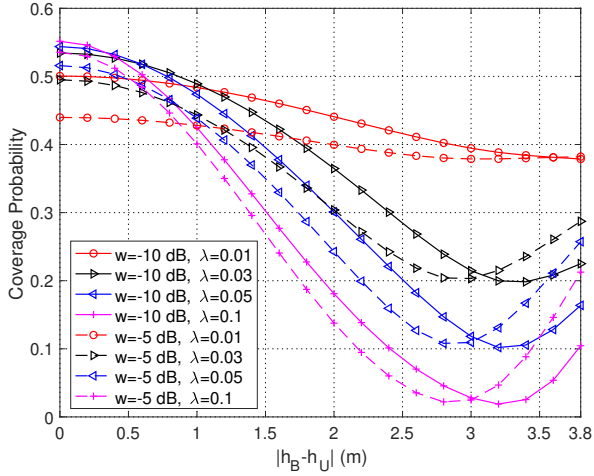


Fig. 3. Coverage probability vs. the absolute value of the height difference between BSs and UEs for different values of w and λ (BS/m²).

Proof: See Appendix C. ■

The area spectral efficiency in bps/Hz/m² can be computed as [34]

$$\mathcal{R}^{\text{ASE}} = \lambda \mathcal{R}, \quad (28)$$

where λ is the density of the BSs in BSs/m² and \mathcal{R} is given in (21).

TABLE II
VALUES OF PARAMETERS

Parameter	Default Value
Path loss at reference distance β_0	-38.5 dB
AWGN average power N	-104 dBm
Coverage probability threshold T	0 dB
Transmit power of BSs P	33 dBm
Path loss exponent α	4
BS height h_B and UE height h_U	1.2 m
Storey height H	3 m
BS density on each storey λ	10^{-2} BS/m ²
Ceiling penetration loss w	-10 dB

V. NUMERICAL RESULTS

In this section, we evaluate the accuracy of our analytical expressions and further analyze the performance of our multi-storey SCN model.

A. Validation of the Analytical Results

For numerical evaluation and simulations, the default values of parameters are listed in Table II [20] unless otherwise stated. As shown in Table 3 of [36], the penetration loss of one ceiling ranges from -4 dB to -22 dB, depending on the carrier frequencies (0.9-5.8 GHz) and building environments. Without loss of generality, we set the default ceiling penetration loss as -10 dB.

In Fig. 2, we compare the coverage probability of the proposed SCN model for $M = 0, 1, 2$ and 3. The analytic curves match well with those simulated by Monte Carlo methods, which demonstrates the accuracy of our mathematical

derivations. In Fig. 2(a)-(d), we can observe that the $M = 0$ case provides the upper bound of the coverage probability where the BS deployment follows the traditional 2D PPP distribution [18]. From Fig. 2(a) and Fig. 2(b), it is obvious that when $w = -5$ dB, the coverage probability of the $M = 0$ case is much higher than that of the $M \geq 1$ cases. However, the performance of the $M = 1$ case is close to $M = 2$ and $M = 3$ cases, the gap between them is up to 0.02 and thus negligible. Additionally, when $w = -10$ dB, the $M = 1$ case shows nearly the same coverage probability as the $M = 2$ and $M = 3$ cases. Similar phenomenon can be observed in Fig. 2(c) and Fig. 2(d), where different values of H and λ are included in the comparison.

Based on the results in Fig. 2, it is reasonable to approximate the proposed multi-storey SCN model for $M = 2, 3$ using the $M = 1$ case, the expressions of which can be found in Proposition 1. Accordingly, we will adopt the analytical results of the $M = 1$ case in the discussions hereafter.

In Fig. 3, we evaluate the impact of the absolute value of the height difference between BSs and UEs on the coverage probability for various values of the ceiling penetration loss and the BS density on each storey through Monte Carlo simulations. We fix the UE height as 1.2 m and set the maximum BS height as 5 m following a practical upper bound of storey height [38]. We can see that the maximum coverage probability is achieved when the BS height is the same as the UE height. Therefore, in the following, we assume that the BS height and the UE height are identical to evaluate the optimal achievable network performance of our proposed multi-storey SCN model.

In Fig. 4, we plot the coverage probability versus the SINR threshold for different values of the BS transmit power, BS density on each storey, ceiling penetration loss, and height of each storey. We can see that the coverage probability does not change with the BS transmit power, for given BS density on each storey, ceiling penetration loss and height of each storey. This is mainly due to the relatively high indoor BS density that leads to an interference-limited multi-storey SCN.

B. Effect of the BS Density

To better demonstrate the performance of the multi-storey SCN, we ignore the thermal noise and set w as -10 dB. It is well-known that the BS density does not affect the network coverage probability in interference-limited networks and the area spectral efficiency scales linearly with the network densification [18]. This is because the increased interference can be compensated by the shrunk distance between the typical UE and the connected BS.

However, we observe a different scaling law in our proposed multi-storey SCN model. In Fig. 5, we analyze the influence of the BS density per storey to the coverage probability for $H = 3$ m, $H = 4$ m, $H = 5$ m [38], [39], respectively. Note that the $M = 0$ curve stands for the 2D scenario [18] and its coverage probability $\mathcal{C}^{M=0}$ remains unchanged with the increase of the BS density. When $M = 1$, the coverage probability first decreases from $\mathcal{C}^{M=0}$ and then increases back to $\mathcal{C}^{M=0}$ with the network densification. This phenomenon

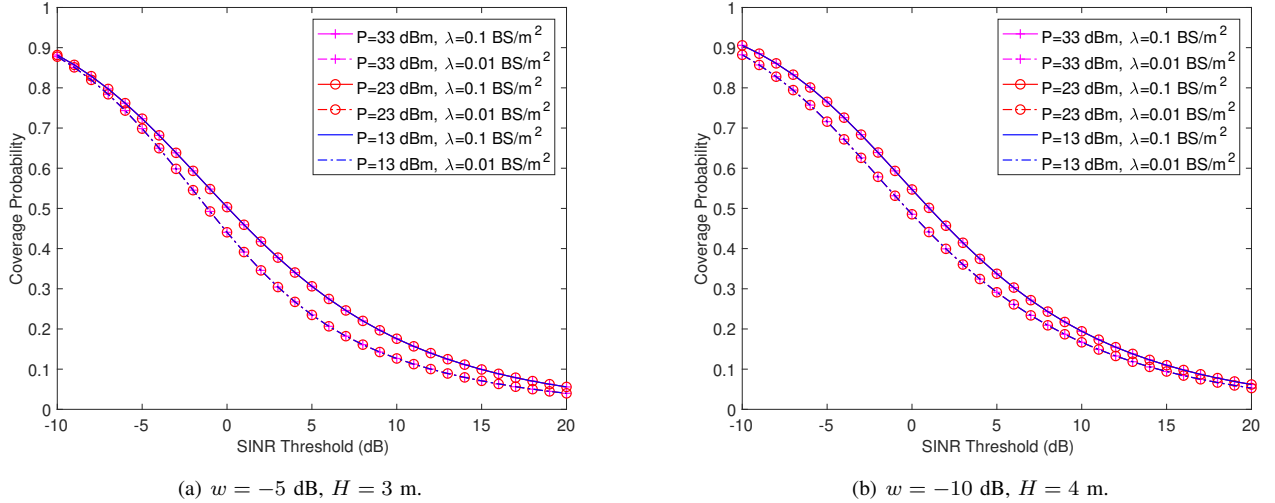


Fig. 4. Coverage probability vs. the SINR threshold for different values of P and λ .

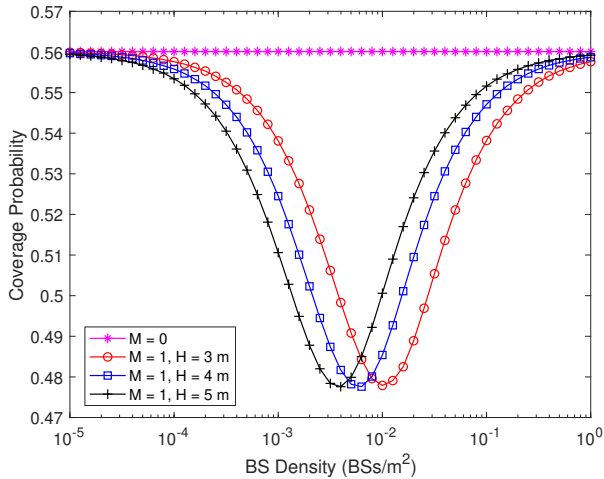


Fig. 5. The coverage probability vs. the BS density.

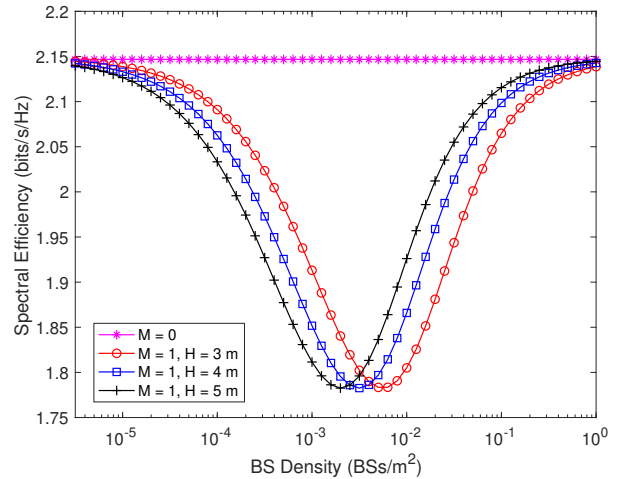


Fig. 6. The spectral efficiency vs. the BS density.

is referred to as the *Coverage Probability Chasm* hereafter. Intuitively, when λ approaches infinity, the typical UE will hardly associate with any storey other than the 0th storey, and thus the coverage probability of the $M > 1$ cases is close to that of the $M = 0$ case. Moreover, the coverage probability as $\lambda \rightarrow 0$ is in accordance with Lemma 2. The minimum value of coverage probability and the corresponding BS density per storey λ^* can be obtained when $\mathcal{C}^{M=1}(\lambda^*) = 0$. The solution can be numerically found using Newton's method, and details are given in Appendix D. The numerical results are 10.476×10^{-3} BS/m², 5.9×10^{-3} BS/m², 3.8×10^{-3} BS/m² for $H = 3$ m, $H = 4$ m, $H = 5$ m, respectively, and the minimum coverage probability is 0.4775. The results reveal that the worst BS densities suffer from more than 8 percent loss of coverage probability compared with the 2D model. Since the spectral efficiency is the integral of the coverage probability, a *SE Chasm* can also be found in Fig. 6, where the worst BS densities can be similarly obtained with Newton's method. The

numerical results are 5.6×10^{-3} BSs/m², 3.1×10^{-3} BSs/m², 2×10^{-3} BSs/m² for $H = 3$ m, $H = 4$ m, $H = 5$ m, respectively, and the minimum spectral efficiency is 1.7826 bps/Hz/m². To alleviate the performance loss, it is necessary to avoid the Chasm area in the practical deployment of BSs.

In Fig. 7, we show the area spectral efficiency of $M = 0$ and $M = 1$ cases. For the $M = 0$ scenario, the ASE increases linearly with network densification. Nevertheless, for the multi-storey case, the ASE first increases linearly when the BS density per storey is low and then exhibits a slowing-down in the ASE growth when the network becomes denser. When the network is ultra dense, the ASE returns to the linear growth again. Such a trend of the ASE performance is not difficult to explain according to the SE trend in Fig. 6. Moreover, we observe that for a given storey height, a higher penetration loss of the ceiling leads to a higher ASE.

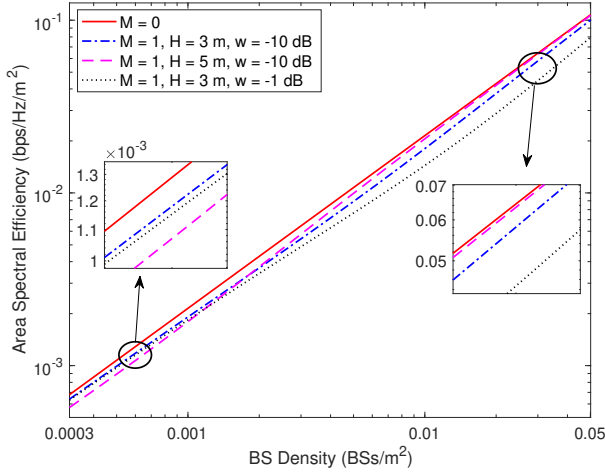


Fig. 7. The area spectral efficiency vs. the BS density.

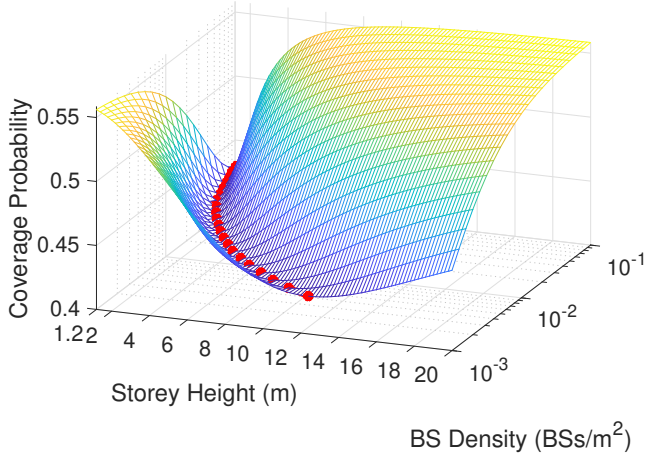


Fig. 8. Coverage probability vs. the storey height H and BS density for $w = -5$ dB. The red bold line shows the storey height and BS density corresponding to the lowest coverage probability.

C. Effect of the Storey Height

In Fig. 8, we assume that the penetration loss of the ceiling $w = -5$ dB, and the threshold of the coverage probability is 0 dB. We assume that the BS height and UE height are both 1.2 m, so the minimum storey height is 1.2 m. We plot the 3D figure to show the influence of the storey height with different BS densities, where a conspicuous *Coverage Probability Chasm* can be observed. For most of the BS densities, the coverage probability of the typical UE first decreases and then increases with the increasing storey height. The red bold line shows the locations of the storey height H^* corresponding to the lowest coverage probability, which can be obtained by solving $C^{M=1'}(H^*) = 0$ and numerically found using a standard bisection searching [40]. Due to the existing of the *Coverage Probability Chasm*, there is a worst storey height that leads to the lowest coverage probability. The worst storey height is affected by the BS density, as can be seen, when the BS density increases, the worst storey height

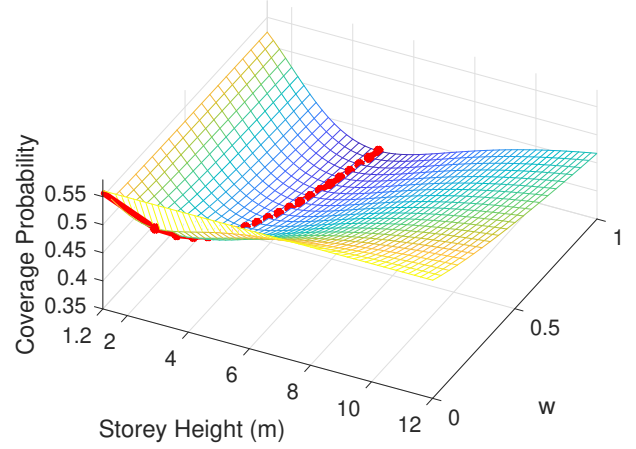


Fig. 9. Coverage probability vs. the storey height H and the ceiling penetration loss w . The red bold line shows the storey height and ceiling penetration loss corresponding to the lowest coverage probability.

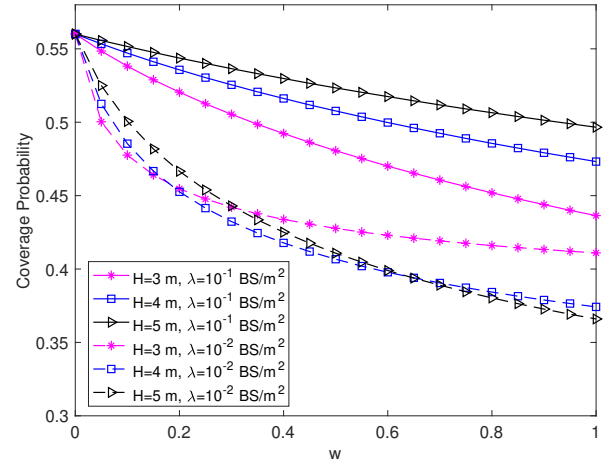


Fig. 10. The coverage probability vs. the ceiling penetration loss w .

decreases. It is worth noting that the coverage probability monotonously increases when the worst storey height is less than 1.2 m.

In Fig. 9, the BS density per storey is set to be 10^{-2} BS/m² and the threshold of the coverage probability is 0 dB. A similar *Coverage Probability Chasm* can be observed. The coverage probability of the typical UE first decreases and then increases with the increasing storey height for a particular penetration loss of the ceiling. The red bold line also indicates the locations of the storey height H^* with lowest coverage probability. Note that a smaller value of w means a higher penetration loss of the ceiling, which indicates that the storey height corresponding to the lowest coverage probability is smaller when the penetration loss becomes higher.

In conclusion, the *Coverage Probability Chasm* exists for any BS density and penetration loss of the ceiling, which is in accordance with the conclusion in Lemma 3. Intuitively, when the storey height is 0, all the BSs are on the same storey, that is the 2D BS deployment. When the storey height

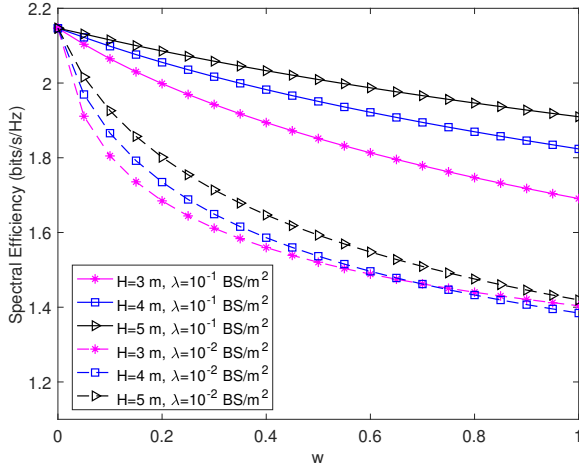


Fig. 11. The spectral efficiency vs. the ceiling penetration loss w .

becomes large enough, the probability of the typical UE being connected to any storey other than the 0th storey is close to 0 and the coverage probability of the $M > 1$ cases is close to that of the 2D model. For the commercial success of future 5G networks, it is crucial to avoid the *Coverage Probability Chasm* in the design of new buildings. Actually, with our tractable expressions, it is convenient to find the optimal storey height. With the acceptable range of storey height, e.g. $H_1 \leq H \leq H_2$, the maximum coverage probability can be obtained at either H_1 or H_2 due to the *Coverage Probability Chasm*. Therefore, we only need to compute the coverage probability at H_1 and H_2 respectively and choose the higher one.

D. Effect of the Penetration Loss of the Ceiling

In Fig. 10 and Fig. 11, we analyze the influence of the penetration loss of the ceiling (in linear scale). Larger w means smaller penetration loss. It is observed that the coverage probability and spectral efficiency increase with stronger penetration loss, which indicates that the cross-storey communication is harmful to the network performance when the BSs and UEs share the same height. When $w = 0$, the typical UE only connects to the BSs on the 0th storey, so the network performance is the same with the 2D model. According to this conclusion, we should choose the materials with higher penetration loss for the ceilings of a new building.

VI. CONCLUSIONS

In this paper, we have proposed a new 3D stochastic geometry model for the small-cell networks in the multi-storey built environment. A novel theoretical discovery has been presented, i.e., the *Coverage Probability Chasm*. The coverage probability first decreases and then increases with the increase of the storey height and the network density. Moreover, we show that a ceilings with a higher penetration loss can provide a better network performance. The contributions of this paper can shed insight on the design of new buildings and future indoor SCN deployments.

In the future, we will further consider a more practical indoor built environment with walls and stochastic blockages. In addition, interference management techniques such as dynamic power control, BS sleeping strategy, and directional antennas will be investigated.

APPENDIX A PROOF OF LEMMA 1

Denote n as the index of the storey that the typical UE connected to. Given the condition that the typical UE is associated to the BS on the m th storey, $X_m > x$ is equal to $R_m > x$, the probability of $X_m > x$ can be computed as

$$\mathbb{P}[X_m > x] = \mathbb{P}[R_m > x | n = m] = \frac{\mathbb{P}[R_m > x, n = m]}{\mathbb{P}[n = m]}, \quad (29)$$

where

$$\mathbb{P}[n = m] = \mathcal{B}_m = \mathbb{E}_{R_m} \left[\mathbb{P} \left[P_{r,m}(R_m) > \max_{j,j \neq m} P_{r,j} \right] \right], \quad (30)$$

the joint probability of $R_m > x$ and $n = m$ is

$$\begin{aligned} & \mathbb{P}[R_m > x, n = m] \\ &= \mathbb{P} \left[R_m > x, P_{r,m}(R_m) > \max_{j,j \neq m} P_{r,j} \right] \\ &= \int_x^\infty \prod_{j=-M, j \neq m}^M \mathbb{P}[P_{r,m}(r) > P_{r,j}] f_{R_m}(r) dr, \end{aligned} \quad (31)$$

from (2), we have

$$\begin{aligned} & \mathbb{P}[P_{r,m}(r) > P_{r,j}] \\ &= \mathbb{P} \left[(m^2 H^2 + r^2)^{-\frac{\alpha}{2}} w^m > (j^2 H^2 + R_j^2)^{-\frac{\alpha}{2}} w^{|j|} \right] \\ &= \mathbb{P} \left[R_j^2 > (m^2 H^2 + r^2) w^{\frac{2(|j|-m)}{\alpha}} - j^2 H^2 \right], \end{aligned} \quad (32)$$

when $|j| \leq m$, $((m^2 H^2 + r^2) w^{\frac{2(|j|-m)}{\alpha}} - j^2 H^2)$ is non-negative, while when $|j| > m$, it could be a negative number. So $\mathbb{P}[P_{r,m}(r) > P_{r,j}]$ can be divided into two parts as

$$\mathbb{P}[P_{r,m}(r) > P_{r,j}] = \begin{cases} \mathbb{P}[P_{r,m}(r) > P_{r,j}], & |j| \leq m \\ \mathbb{P}[P_{r,m}(r) > P_{r,j}], & |j| > m \end{cases} \quad (33)$$

since R_j^2 is always non-negative, so in the case of $|j| > m$, when $(m^2 H^2 + r^2) w^{\frac{2(|j|-m)}{\alpha}} < j^2 H^2$, $\mathbb{P}[P_{r,m}(r) > P_{r,j}]$ is 1. With these analysis, (33) can be further derived as (34), (35).

$$\begin{aligned} & \mathbb{P}[P_{r,m}(r) > P_{r,j}] \\ & \quad |j| \leq m \\ &= \mathbb{P} \left[R_j > \sqrt{(m^2 H^2 + r^2) w^{\frac{2(|j|-m)}{\alpha}} - j^2 H^2} \right] \\ & \stackrel{(a)}{=} \mathbb{P} \left[\text{No BS closer than } \sqrt{(m^2 H^2 + r^2) w^{\frac{2(|j|-m)}{\alpha}} - j^2 H^2} \right] \\ &= \exp \left\{ -\pi \lambda \left((m^2 H^2 + r^2) w^{\frac{2(|j|-m)}{\alpha}} - j^2 H^2 \right) \right\}, \end{aligned} \quad (34)$$

in (34), (a) can be derived from the null probability of a 2D Poisson point process in an area A is $\exp(-\lambda A)$ [18].

$f_{R_m}(r)$ is given from

$$f_{R_m}(r) = \frac{d(1 - \mathbb{P}[R_m > r])}{dr} = e^{-\pi\lambda r^2} 2\pi\lambda r. \quad (36)$$

Since $\mathbb{P}[X_m > x]$ is the CCDF of X_m , the PDF of X_m is

$$\begin{aligned} f_{X_m}(x) &= \frac{d(1 - \mathbb{P}[X_m > x])}{dx} \\ &= \frac{1}{\mathcal{B}_m} \prod_{j=-M, j \neq m}^M \mathbb{P}[P_{r,m}(x) > P_{r,j}] f_{R_m}(x), \end{aligned} \quad (37)$$

Combining (34), (35), (36), (37), we can obtain (38), where (a), (b) can be computed using the sum of a geometric series, $I_{m,k}$, F_m , $F_{m,k}$ are defined in (4), (6), (7), which concludes our proof.

APPENDIX B PROOF OF THEOREM 1

From (10), when the typical UE is associated to the BS on the m th storey, the coverage probability is

$$\mathcal{C}_m = \int_{x=0}^{\infty} \mathbb{P}[\text{SINR}_m(x) > T] f_{X_m}(x) dx, \quad (39)$$

where $f_{X_m}(x)$ is given in (38). Rewrite the $\text{SINR}_m(x)$ as $\gamma_m(x) = \frac{g_{m,0}}{P^{-1}(m^2 H^2 + x^2)^{\frac{\alpha}{2}} w^{-m} Q}$, where $Q = \sum_{j=-M}^M I_j +$

N/β_0 . Then $\mathbb{P}[\text{SINR}_m(x) > T]$ can be derived as

$$\begin{aligned} &\mathbb{P}[\text{SINR}_m(x) > T] \\ &= \mathbb{P}\left[g_{m,0} > P^{-1}(m^2 H^2 + x^2)^{\frac{\alpha}{2}} w^{-m} T Q\right] \\ &= \int_0^{\infty} \exp\left\{-P^{-1}(m^2 H^2 + x^2)^{\frac{\alpha}{2}} w^{-m} T Q\right\} f_Q(q) dq \\ &= \mathbb{E}_Q\left[\exp\left\{-P^{-1}(m^2 H^2 + x^2)^{\frac{\alpha}{2}} w^{-m} T Q\right\}\right] \\ &= \exp\left\{-\frac{T}{\text{SNR}_m}\right\} \prod_{j=-M}^M \mathcal{L}_{I_j}\left(P^{-1}(m^2 H^2 + x^2)^{\frac{\alpha}{2}} w^{-m} T\right), \end{aligned} \quad (40)$$

where SNR_m is given in (14), define $l_{m,x} = \sqrt{m^2 H^2 + x^2}$, $l_{j,y} = \sqrt{j^2 H^2 + y^2}$, the Laplace transform of I_j is

$$\begin{aligned} &\mathcal{L}_{I_j}(P^{-1} l_{m,x}^{\alpha} w^{-m} T) \\ &= \mathbb{E}_{I_j}\left[\exp\left\{-P^{-1} l_{m,x}^{\alpha} w^{-m} T I_j\right\}\right] \\ &= \mathbb{E}_{\Phi_j}\left[\exp\left\{-l_{m,x}^{\alpha} T \sum_{i \in \Phi_j} h_{j,i} l_{j,y}^{-\alpha} w^{|j|-m}\right\}\right] \\ &\stackrel{(a)}{=} \exp\left\{-2\pi\lambda \int_{z_j}^{\infty} \left(1 - \mathcal{L}_{h_j}(l_{m,x}^{\alpha} T l_{j,y}^{-\alpha} w^{|j|-m})\right) y dy\right\} \\ &\stackrel{(b)}{=} \exp\left\{-2\pi\lambda \int_{z_j}^{\infty} \left(1 - \frac{1}{1 + l_{m,x}^{\alpha} T l_{j,y}^{-\alpha} w^{|j|-m}}\right) y dy\right\} \\ &= \exp\left\{-2\pi\lambda \int_{z_j}^{\infty} \frac{y}{1 + l_{m,x}^{\alpha} T^{-1} w^{m-|j|} l_{j,y}^{\alpha}} dy\right\}, \end{aligned} \quad (41)$$

where (a) comes from the probability generating functional of PPP [33], and (b) is because $h_j \sim \exp(1)$. z_j is the horizontal

$$\begin{aligned} \mathbb{P}[P_{r,m}(r) > P_{r,j}] &= \begin{cases} 1, & r < \sqrt{j^2 H^2 w^{\frac{2(m-|j|)}{\alpha}} - m^2 H^2} \\ \mathbb{P}\left[R_j > \sqrt{(m^2 H^2 + r^2) w^{\frac{2(|j|-m)}{\alpha}} - j^2 H^2}\right], & r \geq \sqrt{j^2 H^2 w^{\frac{2(m-|j|)}{\alpha}} - m^2 H^2} \end{cases} \\ &= \begin{cases} 1, & r < \sqrt{j^2 H^2 w^{\frac{2(m-|j|)}{\alpha}} - m^2 H^2} \\ \exp\left\{-\pi\lambda \left((m^2 H^2 + r^2) w^{\frac{2(|j|-m)}{\alpha}} - j^2 H^2\right)\right\}, & r \geq \sqrt{j^2 H^2 w^{\frac{2(m-|j|)}{\alpha}} - m^2 H^2} \end{cases} \end{aligned} \quad (35)$$

$$\begin{aligned} f_{X_m}(x) &= \frac{2\pi\lambda}{\mathcal{B}_m} x \exp\left\{-\pi\lambda x^2\right\} \prod_{-m \leq j < m} \mathbb{P}[P_{r,m}(x) > P_{r,j}] \prod_{m < |j| \leq M} \mathbb{P}[P_{r,m}(x) > P_{r,j}] \\ &= \frac{2\pi\lambda}{\mathcal{B}_m} x \exp\left\{-\pi\lambda x^2\right\} \exp\left\{-\pi\lambda \sum_{-m \leq j < m} \left((m^2 H^2 + x^2) w^{\frac{2(|j|-m)}{\alpha}} - j^2 H^2\right)\right\} \prod_{m < |j| \leq M} \mathbb{P}[P_{r,m}(x) > P_{r,j}] \\ &\stackrel{(a)}{=} \frac{2\pi\lambda}{\mathcal{B}_m} x \exp\left\{-\pi\lambda F_m\right\} \prod_{m < |j| \leq M} \mathbb{P}[P_{r,m}(x) > P_{r,j}] \\ &\stackrel{(b)}{=} \begin{cases} \frac{2\pi\lambda}{\mathcal{B}_m} x \exp\left\{-\pi\lambda(F_m + F_{m,m})\right\}, & 0 < x \leq I_{m,(m+1)} \\ \dots \\ \frac{2\pi\lambda}{\mathcal{B}_m} x \exp\left\{-\pi\lambda(F_m + F_{m,k})\right\}, & I_{m,k} < x \leq I_{m,(k+1)} \\ \dots \\ \frac{2\pi\lambda}{\mathcal{B}_m} x \exp\left\{-\pi\lambda(F_m + F_{m,M})\right\}, & I_{m,M} < x < \infty \end{cases} \end{aligned} \quad (38)$$

distance of the closest interfering BS on the j th storey, similar with (33), it is derived as

$$z_j = \begin{cases} z_j, & |j| \leq m \\ z_j, & |j| > m \end{cases} \quad (42)$$

where

$$z_j = \sqrt{(m^2 H^2 + x^2) w^{\frac{2(|j|-m)}{\alpha}} - j^2 H^2}, \quad |j| \leq m \quad (43)$$

$$z_j = \begin{cases} 0, & x < I_{m,|j|} \\ \sqrt{(m^2 H^2 + x^2) w^{\frac{2(|j|-m)}{\alpha}} - j^2 H^2}, & x \geq I_{m,|j|} \end{cases} \quad |j| > m \quad (44)$$

where $I_{m,|j|}$ can be computed using (4). Then $\mathcal{L}_{I_j}(P^{-1}l_{m,x}^\alpha w^{-m}T)$ can be derived as

$$\mathcal{L}_{I_j}(P^{-1}l_{m,x}^\alpha w^{-m}T) = \begin{cases} \mathcal{L}_{I_j}(P^{-1}l_{m,x}^\alpha w^{-m}T), & |j| \leq m \\ \mathcal{L}_{I_j}(P^{-1}l_{m,x}^\alpha w^{-m}T), & |j| > m \end{cases} \quad (45)$$

employ a change of variable $u = (l_{j,y}^{-\alpha} l_{m,x}^\alpha T w^{|j|-m})^{-2/\alpha}$, we can obtain

$$\mathcal{L}_{I_j}(P^{-1}l_{m,x}^\alpha w^{-m}T) = \exp\left\{-\pi\lambda Q_{m,x}^2 w^{\frac{2(|j|-m)}{\alpha}}\right\}, \quad |j| \leq m \quad (46)$$

where

$$Q = T^{\frac{2}{\alpha}} \int_{T^{-\frac{2}{\alpha}}}^{\infty} \frac{1}{1+u^{\frac{\alpha}{2}}} du = \frac{2T}{\alpha-2} {}_2F_1\left[1, 1 - \frac{2}{\alpha}; 2 - \frac{2}{\alpha}; -T\right] \text{ for } \alpha > 2, \quad (47)$$

here ${}_2F_1[\cdot]$ denotes the Gauss hypergeometric function. For $|j| > m$,

$$\begin{aligned} & \mathcal{L}_{I_j}(P^{-1}l_{m,x}^\alpha w^{-m}T) \\ &= \begin{cases} \exp\left\{-\pi\lambda Q_{m,|j|} l_{m,x}^2 w^{\frac{2(|j|-m)}{\alpha}}\right\}, & x < I_{m,|j|} \\ \exp\left\{-\pi\lambda Q_{m,x}^2 w^{\frac{2(|j|-m)}{\alpha}}\right\}, & x \geq I_{m,|j|} \end{cases} \end{aligned} \quad (48)$$

where

$$\begin{aligned} Q_{m,|j|} &= T^{\frac{2}{\alpha}} \int_{\frac{w^{\frac{2(|j|-m)}{\alpha}} (|j|H)^2}{(m^2 H^2 + x^2) T^{\frac{2}{\alpha}}}}^{\infty} \frac{1}{1+u^{\frac{\alpha}{2}}} du, \\ &= \frac{2TB_{m,|j|,x}^{2/\alpha-1}}{\alpha-2} {}_2F_1\left[1, 1 - \frac{2}{\alpha}; 2 - \frac{2}{\alpha}; -\frac{T}{B_{m,|j|,x}}\right], \end{aligned} \quad (49)$$

where $B_{m,|j|,x} = (|j|H)^\alpha w^{m-|j|} (m^2 H^2 + x^2)^{-\frac{\alpha}{2}}$. Plug (46), (48) into (40), we have (50), in which $D_{m,k} = \sum_{n=1}^M Q_{m,n,k} w^{\frac{2}{\alpha}(n-m)}$, $Q_{m,n,k}$ is given in (16). Combining (38), (39), (50), we can get the coverage probability for the m th storey in (12).

APPENDIX C PROOF OF THEOREM 2

From (23), the average ergodic rate of the typical UE when it is associated to the BS on the m th storey is

$$\mathcal{R}_m = \int_0^\infty \mathbb{E}_{\text{SINR}_m} [\log_2(1 + \text{SINR}_m(x))] f_{X_m}(x) dx, \quad (51)$$

$$\begin{aligned} \mathbb{P}[\text{SINR}_m(x) > T] &= \exp\left\{-\frac{T}{\text{SINR}_m}\right\} \prod_{|j| \leq m} \mathcal{L}_{I_j}(P^{-1}l_{m,x}^\alpha w^{-m}T) \prod_{m < |j| \leq M} \mathcal{L}_{I_j}(P^{-1}l_{m,x}^\alpha w^{-m}T) \\ &= \exp\left\{-\frac{T}{\text{SINR}_m}\right\} \exp\left\{\sum_{j=-m}^m -\pi\lambda Q_{m,x}^2 w^{\frac{2(|j|-m)}{\alpha}}\right\} \prod_{m < |j| \leq M} \mathcal{L}_{I_j}(P^{-1}l_{m,x}^\alpha w^{-m}T) \\ &= \begin{cases} \exp\left\{-\frac{T}{\text{SINR}_m} - \pi\lambda Q(m^2 H^2 + x^2) w^{-\frac{2m}{\alpha}} - 2\pi\lambda(m^2 H^2 + x^2) D_{m,m}\right\}, & 0 < x \leq I_{m,(m+1)} \\ \dots \\ \exp\left\{-\frac{T}{\text{SINR}_m} - \pi\lambda Q(m^2 H^2 + x^2) w^{-\frac{2m}{\alpha}} - 2\pi\lambda(m^2 H^2 + x^2) D_{m,k}\right\}, & I_{m,k} < x \leq I_{m,(k+1)} \\ \dots \\ \exp\left\{-\frac{T}{\text{SINR}_m} - \pi\lambda Q(m^2 H^2 + x^2) w^{-\frac{2m}{\alpha}} - 2\pi\lambda(m^2 H^2 + x^2) D_{m,M}\right\}, & I_{m,M} < x < \infty \end{cases} \end{aligned} \quad (50)$$

$\mathbb{E}_{\text{SINR}_m} [\log_2(1 + \text{SINR}_m(x))]$

$$\begin{aligned} &= \begin{cases} \int_0^\infty \exp\left\{-\frac{2^t-1}{\text{SINR}_m} - \pi\lambda Q_t(m^2 H^2 + x^2) w^{-\frac{2m}{\alpha}} - 2\pi\lambda(m^2 H^2 + x^2) D_{m,m,t}\right\} dt, & 0 < x \leq I_{m,(m+1)} \\ \dots \\ \int_0^\infty \exp\left\{-\frac{2^t-1}{\text{SINR}_m} - \pi\lambda Q_t(m^2 H^2 + x^2) w^{-\frac{2m}{\alpha}} - 2\pi\lambda(m^2 H^2 + x^2) D_{m,k,t}\right\} dt, & I_{m,k} < x \leq I_{m,(k+1)} \\ \dots \\ \int_0^\infty \exp\left\{-\frac{2^t-1}{\text{SINR}_m} - \pi\lambda Q_t(m^2 H^2 + x^2) w^{-\frac{2m}{\alpha}} - 2\pi\lambda(m^2 H^2 + x^2) D_{m,M,t}\right\} dt, & I_{m,M} < x < \infty \end{cases} \end{aligned} \quad (53)$$

where $f_{X_m}(x)$ can be found in Lemma 1. For a positive random variable X , $\mathbb{E}[X] = \int_0^\infty \mathbb{P}[X > x] dx$, define $l_{m,x} = \sqrt{m^2 H^2 + x^2}$, we obtain

$$\begin{aligned} & \mathbb{E}_{\text{SINR}_m} [\log_2(1 + \text{SINR}_m(x))] \\ &= \int_0^\infty \mathbb{P}[\log_2(1 + \text{SINR}_m(x)) > t] dt \\ &\stackrel{(a)}{=} \int_0^\infty \mathbb{P}[g_{m,0} > P^{-1} l_{m,x}^\alpha w^{-m} (2^t - 1) Q] dt \\ &= \int_0^\infty e^{-\frac{2^t - 1}{\text{SINR}_m}} \prod_{j=-M}^M \mathcal{L}_{I_j}(P^{-1} l_{m,x}^\alpha w^{-m} (2^t - 1)) dt, \end{aligned} \quad (52)$$

where (a) comes from employ $T = 2^t - 1$ in (40). Following the derivation in (50), (52) can be further derived as (53), in which

$$\begin{aligned} \mathcal{Q}_t &= (2^t - 1)^{\frac{2}{\alpha}} \int_{(2^t - 1)^{-\frac{2}{\alpha}}}^\infty \frac{1}{1 + u^{\frac{\alpha}{2}}} du \\ &= \frac{2(2^t - 1)}{\alpha - 2} {}_2F_1\left[1, 1 - \frac{2}{\alpha}; 2 - \frac{2}{\alpha}; 1 - 2^t\right], \end{aligned} \quad (54)$$

and $D_{m,k,t} = \sum_{n=1}^M \mathcal{Q}_{m,n,k,t} w^{\frac{2}{\alpha}(n-m)}$, $\mathcal{Q}_{m,n,k,t}$ is given in (27). Plug (53) into (51), we can get the expression in (22).

APPENDIX D

PROOF OF NEWTON'S METHOD

To obtain the minimum value of coverage probability and the corresponding BS density per storey in (17), we employ the Newton's method. Assume that λ is the only variable, the coverage probability is

$$\mathcal{C}^{M=1}(\lambda) = \mathcal{B}_0 \mathcal{C}_0 + 2\mathcal{B}_1 \mathcal{C}_1 \quad (55)$$

where $\mathcal{B}_0 \mathcal{C}_0$ and $\mathcal{B}_1 \mathcal{C}_1$ can be found in (18), (19). Take the first-order derivation of $\mathcal{C}^{M=1}(\lambda)$ and we have

$$\begin{aligned} \mathcal{C}^{M=1'}(\lambda) &= \frac{-\pi \mathcal{P} H^2}{1 + \mathcal{Q}} \exp\{-\pi \lambda \mathcal{P} H^2\} \\ &+ \int_0^{Hw^{-\frac{1}{\alpha}}} 2\pi x (1 - \pi \lambda \mathcal{K} x^2) \exp\{-\pi \lambda \mathcal{K} x^2\}, \end{aligned} \quad (56)$$

where $\mathcal{P} = \mathcal{Q} \left(2 + w^{-\frac{2}{\alpha}}\right) + w^{-\frac{2}{\alpha}}$, $\mathcal{K} = 1 + \mathcal{Q} + 2\mathcal{Q}_{0,1} w^{\frac{2}{\alpha}}$, \mathcal{Q} and $\mathcal{Q}_{0,1}$ are defined in (15) and (20). Then take the second-order derivation of $\mathcal{C}^{M=1}(\lambda)$ and we have

$$\begin{aligned} \mathcal{C}^{M=1''}(\lambda) &= \frac{\pi^2 \mathcal{P}^2 H^4}{1 + \mathcal{Q}} \exp\{-\pi \lambda \mathcal{P} H^2\} \\ &+ \int_0^{Hw^{-\frac{1}{\alpha}}} (2\lambda \mathcal{K}^2 \pi^3 x^5 - 4\mathcal{K} \pi^2 x^3) \exp\{-\pi \lambda \mathcal{K} x^2\}. \end{aligned} \quad (57)$$

Our objective is to find the λ^* when $\mathcal{C}^{M=1'}(\lambda^*) = 0$. Choose a threshold ε which is close to zero and an initial value λ_0 . In our simulation, we set $\varepsilon = 10^{-6}$ and $\lambda_0 = 0$. Compute λ_1 according to

$$\lambda_{n+1} = \lambda_n - \frac{\mathcal{C}^{M=1'}(\lambda_n)}{\mathcal{C}^{M=1''}(\lambda_n)}, \quad (58)$$

and continue the iteration until $\mathcal{C}^{M=1'}(\lambda_{n+1}) < \varepsilon$. Then we obtain the target BS density per storey $\lambda^* = \lambda_{n+1}$ and the minimum coverage probability $\mathcal{C}^{M=1}(\lambda^*)$.

REFERENCES

- [1] J. G. Andrews *et al.*, "What will 5G be?" *IEEE J. Sel. Areas Commun.*, vol. 32, no. 6, pp. 1065-1082, Jun. 2014.
- [2] "Cisco visual networking index: global mobile data traffic forecast update, 2017-2022," Cisco, San Jose, CA, USA, White Paper, Feb. 2019.
- [3] Huawei. (Feb. 2016). "Five trends to small cell 2020," [Online]. Available: <http://www-file.huawei.com/~media/CORPORATE/PDF/News/Five-Trends-To-Small-Cell-2020-en.pdf>
- [4] J. Zhang and G. d. I. Roche, "Femtocells: technologies and deployment," *John Wiley and Sons*, 2010.
- [5] T. Nakamura *et al.*, "Trends in small cell enhancements in LTE advanced," *IEEE Commun. Mag.*, vol. 51, no. 2, pp. 98-105, Feb. 2013.
- [6] H. S. Dhillon, R. K. Ganti, F. Baccelli, and J. G. Andrews, "Modeling and analysis of K-tier downlink heterogeneous cellular networks," *IEEE J. Sel. Areas Commun.*, vol. 30, no. 3, pp. 550-560, Apr. 2012.
- [7] T. Bai, R. Vaze, and R. W. Heath, "Analysis of blockage effects on urban cellular networks," *IEEE Trans. Wireless Commun.*, vol. 13, no. 9, pp. 5070-5083, Sep. 2014.
- [8] A. Thornburg, T. Bai and R. W. Heath, "Performance analysis of outdoor mmWave ad hoc networks," *IEEE Trans. Signal Process.*, vol. 64, no. 15, pp. 4065-4079, Aug. 2016.
- [9] B. Yang, G. Mao, M. Ding, X. Ge and X. Tao, "Dense small cell networks: from noise-limited to dense interference-limited," *IEEE Trans. Veh. Technol.*, vol. 67, no. 5, pp. 4262-4277, May. 2018.
- [10] X. Wang, E. Turgut and M. C. Gursoy, "Coverage in downlink heterogeneous mmWave cellular networks with user-centric small cell deployment," *IEEE Trans. Veh. Technol.*, vol. 68, no. 4, pp. 3513-3533, Apr. 2019.
- [11] J. Liu, M. Sheng and J. Li, "Improving network capacity scaling law in ultra-dense small cell networks," *IEEE Trans. Wireless Commun.*, vol. 17, no. 9, pp. 6218-6230, Sept. 2018.
- [12] M. K. Muller, M. Tarantetz, and M. Rupp, "Analyzing wireless indoor communications by blockage models," *IEEE Access*, vol. 5, pp. 2172-2186, 2017.
- [13] S. Niknam, B. Natarajan and R. Barazideh, "Interference analysis for finite-area 5G mmWave networks considering blockage effect," *IEEE Access*, vol. 6, pp. 23470-23479, 2018.
- [14] M. K. Müller, S. Schwarz and M. Rupp, "Investigation of area spectral efficiency in indoor wireless communications by blockage models," *International Symposium on Modeling and Optimization in Mobile, Ad Hoc, and Wireless Networks (WiOpt)*, Shanghai, 2018, pp. 1-6.
- [15] H. Zheng, J. Zhang, H. Li, Q. Hong, H. Hu and J. Zhang, "Exact line-of-sight probability for channel modeling in typical indoor environments," *IEEE Antennas Wireless Propag. Lett.*, vol. 17, no. 7, pp. 1359-1362, Jul. 2018.
- [16] K. Venugopal and R. W. Heath, "Location based performance model for indoor mmWave wearable communication," *Proc. of International Conference on Communications (ICC)*, pp. 1-6, IEEE, 2016.
- [17] R. Kovalchukov *et al.*, "Evaluating SIR in 3D millimeter-wave deployments: direct modeling and feasible approximations," *IEEE Trans. Wireless Commun.*, vol. 18, no. 2, pp. 879-896, Feb. 2019.
- [18] J. G. Andrews, F. Baccelli, and R. K. Ganti, "A tractable approach to coverage and rate in cellular networks," *IEEE Trans. Commun.*, vol. 59, no. 11, pp. 3122-3134, Nov. 2011.
- [19] T. Bai and R. W. Heath, Jr., "Coverage and rate analysis for millimeter-wave cellular networks," *IEEE Trans. Wireless Commun.*, vol. 14, no. 2, pp. 1100-1114, Feb. 2015.
- [20] H. Jo, Y. J. Sang, P. Xia and J. G. Andrews, "Heterogeneous cellular networks with flexible cell association: a comprehensive downlink SINR analysis," *IEEE Trans. Wireless Commun.*, vol. 11, no. 10, pp. 3484-3495, Oct. 2012.
- [21] H. Hu, J. Weng and J. Zhang, "Coverage performance analysis of FeICIC low-power subframes," *IEEE Trans. Wireless Commun.*, vol. 15, no. 8, pp. 5603-5614, Aug. 2016.
- [22] H. Hu, Y. Gao, J. Zhang, X. Chu and J. Zhang, "Density analysis of LTE-LAA networks coexisting with WiFi sharing multiple unlicensed channels," *IEEE Access*, vol. 7, pp. 148004-148018, 2019.
- [23] Z. Pan and Q. Zhu, "Modeling and analysis of coverage in 3-D cellular networks," *IEEE Commun. Lett.*, vol. 19, no. 5, pp. 831-834, May. 2015.
- [24] A. K. Gupta, X. Zhang, and J. G. Andrews, "SINR and throughput scaling in ultradense urban cellular networks," *IEEE Wireless Commun. Lett.*, Aug. 2015.
- [25] J. Lee, X. Zhang, and F. Baccelli, "A 3-D spatial model for in-building wireless networks with correlated shadowing," *IEEE Trans. Wireless Commun.*, vol. 15, no. 11, pp. 7778-7793, Nov. 2016.

- [26] J. Liu, T. Kou, Q. Chen and H. D. Sherali, "Femtocell base station deployment in commercial buildings: a global optimization approach," *IEEE J. Sel. Areas Commun.*, vol. 30, no. 3, pp. 652-663, Apr. 2012.
- [27] H.-Y. Hsieh, S.-E. Wei, and C.-P. Chien, "Optimizing small cell deployment in arbitrary wireless networks with minimum service rate constraints," *IEEE Trans. Mobile Comput.*, vol. 13, no. 8, pp. 1801-1815, Aug. 2014.
- [28] M. Lin and T. L. Porta, "Energy-aware enterprise femtocell deployment," *2014 IEEE Wireless Communications and Networking Conference (WCNC)*, Istanbul, 2014, pp. 2312-2317.
- [29] J. G. Andrews, X. Zhang, G. D. Durgin and A. K. Gupta, "Are we approaching the fundamental limits of wireless network densification?" *IEEE Commun. Mag.*, vol. 54, no. 10, pp. 184-190, Oct. 2016.
- [30] J. Liu, M. Sheng, L. Liu and J. Li, "Network densification in 5G: from the short-range communications perspective," *IEEE Commun. Mag.*, vol. 55, no. 12, pp. 96-102, Dec. 2017.
- [31] J. Liu, M. Sheng, L. Liu, and J. Li, "Effect of densification on cellular network performance with bounded pathloss model," *IEEE Commun. Lett.*, vol. 21, no. 2, pp. 346-349, Feb. 2017.
- [32] M. Kamel, W. Hamouda and A. Youssef, "Ultra-dense networks: a survey," *IEEE Commun. Surveys Tut.*, vol. 18, no. 4, pp. 2522-2545, Fourthquarter 2016.
- [33] M. Ding, P. Wang, D. López-Pérez, G. Mao, and Z. Lin, "Performance impact of LoS and NLoS transmissions in dense cellular networks," *IEEE Trans. Wireless Commun.*, vol. 15, no. 3, pp. 2365-2380, Mar. 2016.
- [34] M. Ding and D. López-Pérez, "Performance impact of base station antenna heights in dense cellular networks," *IEEE Trans. Wireless Commun.*, vol. 16, no. 12, pp. 8147-8161, Dec. 2017.
- [35] X. Zhang and J. G. Andrews, "Downlink cellular network analysis with multi-slope path loss models," *IEEE Trans. Commun.*, vol. 63, no. 5, pp. 1881-1894, May. 2015.
- [36] ITU-R Recommendation P.1238-10, "Propagation data and prediction methods for the planning of indoor radio communication systems and radio local area networks in the frequency range 300 MHz to 450 GHz," 2019.
- [37] J. Zhang, A. A. Glazunov and J. Zhang, "Wireless energy efficiency evaluation for buildings under design based on analysis of interference gain," *IEEE Trans. Veh. Tech.*, accepted for publication.
- [38] J. Hygh, J. DeCarolis, D. Hill and R. Ranjithan, "Multivariate regression as an energy assessment tool in early building design," *Build Environ*, vol. 57, pp. 165-175, 2012.
- [39] M. Zhen, Y. Du, F. Hong and G. Bian, "Simulation analysis of natural lighting of residential buildings in Xi'an, China", *Sci Total Environ*, vol. 690, pp. 197-208, 2019.
- [40] R. L. Burden and J. D. Faires, "Numerical analysis (3rd Ed.)," *PWS Publishers*, 1985.



Chen Chen received the B.E. degree from East China University of Science and Technology, Shanghai, China, in 2018. He is currently pursuing his Ph.D. degree at the Department of Electronic and Electrical Engineering, The University of Sheffield, UK. His current research interests include millimeter wave networks, UAV communication, green networks, stochastic geometry and machine learning.



Yixin Zhang received the B.Eng. degree from Beijing University of Posts and Telecommunications, Beijing, China, in 2017. She is currently pursuing the Ph.D. degree in the Department of Electronic and Electrical Engineering at the University of Sheffield, Sheffield, UK. Her research interests include electromagnetic wave propagation, wireless channel modelling, MIMO antenna configurations, and indoor wireless networks.



Jiliang Zhang (M'15, SM'19) received the B.E., M.E., and Ph.D. degrees from the Harbin Institute of Technology, Harbin, China, in 2007, 2009, and 2014, respectively. He was a Postdoctoral Fellow with Shenzhen Graduate School, Harbin Institute of Technology from 2014 to 2016, an Associate Professor with the School of Information Science and Engineering, Lanzhou University from 2017 to 2019, and a researcher at the Department of Electrical Engineering, Chalmers University of Technology, Gothenburg, Sweden from 2017 to 2018. He is now

a Marie Curie Research Fellow at the Department of Electronic and Electrical Engineering, The University of Sheffield, Sheffield, UK. His current research interests include, but are not limited to wireless channel modelling, modulation system, relay system, wireless ranging system, vehicular communications, ultra-dense small cell networks, neural dynamic, and smart environment modelling.



Xiaoli Chu (M'06-SM'15) is a Professor in the Department of Electronic and Electrical Engineering at the University of Sheffield, UK. She received the B.Eng. degree in Electronic and Information Engineering from Xi'an Jiao Tong University in 2001 and the Ph.D. degree in Electrical and Electronic Engineering from the Hong Kong University of Science and Technology in 2005. From 2005 to 2012, she was with the Centre for Telecommunications Research at King's College London. Xiaoli has co-authored over 140 peer-reviewed journal and conference papers and is co-recipient of the IEEE Communications Society 2017 Young Author Best Paper Award. She is the lead editor/author of the book "Heterogeneous Cellular Networks - Theory, Simulation and Deployment" published by Cambridge University Press and the book "4G Femtocells: Resource Allocation and Interference Management" published by Springer. She is Editor for the IEEE Communications Letters and the IEEE Wireless Communications Letters and received the IEEE Communications Letters Editor Award in 2018. She was Guest Editor for the IEEE Transactions on Vehicular Technology and the ACM/Springer Journal of Mobile Networks & Applications. She was Co-Chair of the Wireless Communications Symposium for the IEEE International Conference on Communications (ICC) 2015, and has organized 6 workshops on heterogeneous and small cell networks for IEEE ICC, GLOBECOM, WCNC, and PIMRC.

She is the lead editor/author of the book "Heterogeneous Cellular Networks - Theory, Simulation and Deployment" published by Cambridge University Press and the book "4G Femtocells: Resource Allocation and Interference Management" published by Springer. She is Editor for the IEEE Communications Letters and the IEEE Wireless Communications Letters and received the IEEE Communications Letters Editor Award in 2018. She was Guest Editor for the IEEE Transactions on Vehicular Technology and the ACM/Springer Journal of Mobile Networks & Applications. She was Co-Chair of the Wireless Communications Symposium for the IEEE International Conference on Communications (ICC) 2015, and has organized 6 workshops on heterogeneous and small cell networks for IEEE ICC, GLOBECOM, WCNC, and PIMRC.



Jiliang Zhang is Founder and Chief Scientific Officer (CSO) of Ranplan Wireless (www.ranplanwireless.com), a public company listed on Nasdaq OMX. He has also held the Chair in Wireless Systems at the Department of Electronic and Electrical Engineering, University of Sheffield (www.sheffield.ac.uk) since Jan. 2011. Along with his students and colleagues, he has pioneered research in small cell and heterogeneous network (HetNet) and published some of the landmark papers and book on these topics, widely

used by both academia and industry. With Google scholar citations in excess of 6300, Prof. Zhang is a renowned authority in his field of expertise. In his current roles as CSO at Ranplan and Chair Professor at Sheffield University, Prof. Zhang leads a team of over 30 researchers at PhD candidate level or above. The team has 12 on-going research projects funded by the European Commission and Innovate UK on data-driven proactive network optimisation, millimetre wave small cell communications in the built environments, and modelling and design of smart environments. Prior to his current appointments, he studied and worked at Imperial College London, Oxford University and the University of Bedfordshire, reaching the rank of a Lecturer, Reader and Professor in 2002, 2005 and 2006 respectively.